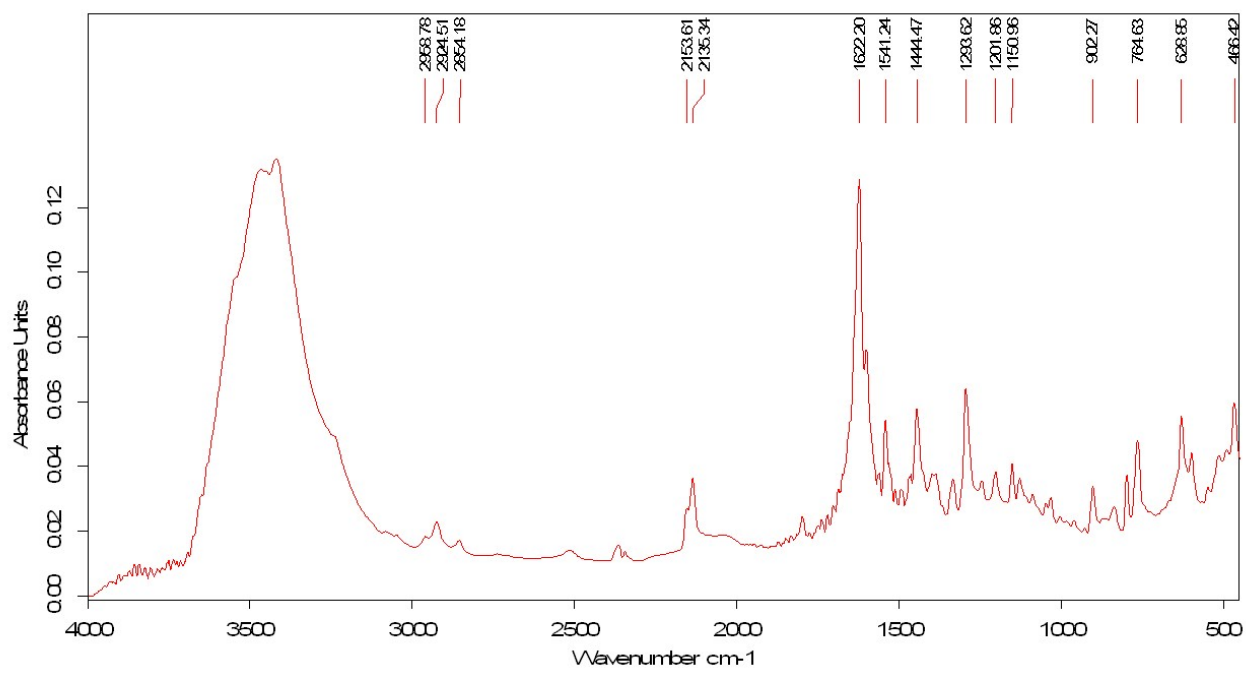


## Electronic Supplementary Information

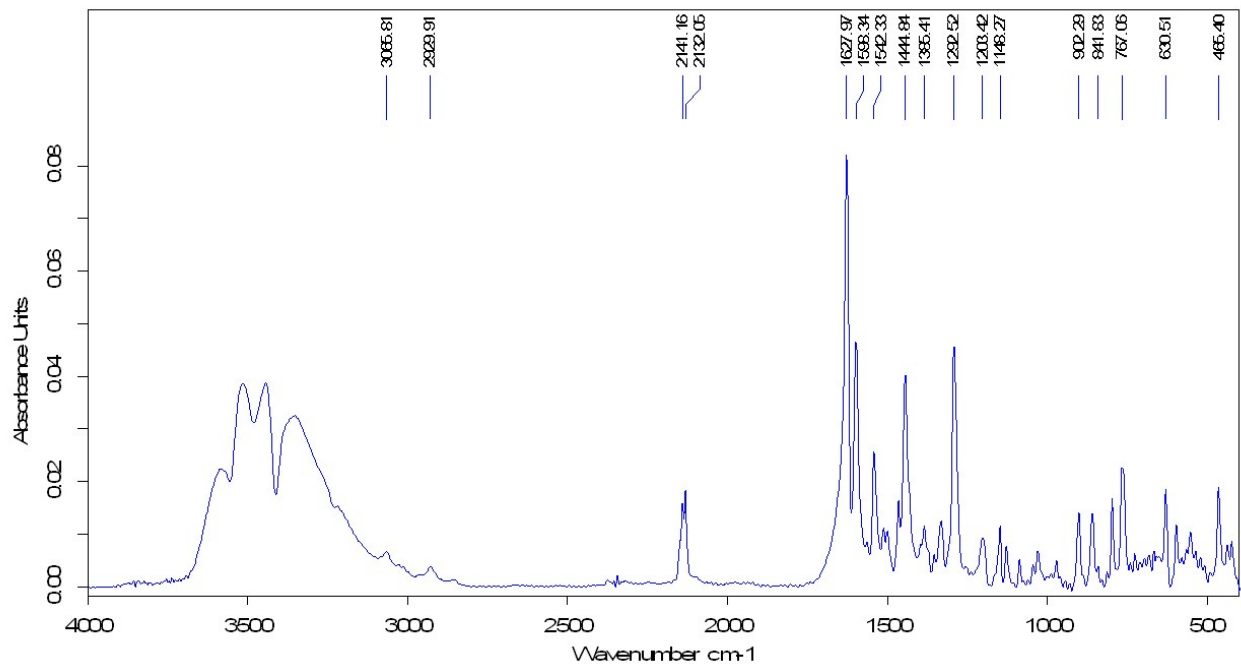
### **{Co<sup>III</sup>Mn<sup>III</sup>}<sub>n</sub> corrugated chains based on heteroleptic cyanido metalloligands**

Maria-Gabriela Alexandru,<sup>a</sup> Diana Visinescu,<sup>b</sup> Nadia Marino,<sup>c</sup> Giovanni De Munno,<sup>c</sup> Francesc Lloret<sup>d</sup> and Miguel Julve<sup>d</sup>

- [a] Department of Inorganic Chemistry, Physical Chemistry and Electrochemistry, Faculty of Applied Chemistry and Materials Science, University “Politehnica” of Bucharest, 1-7 Gh. Polizu Street, 011061 Bucharest, Romania, E-mail address: alexandru.gabriela@gmail.com
- [b] Coordination and Supramolecular Chemistry Laboratory, “Ilie Murgulescu” Institute of Physical Chemistry, Romanian Academy, Splaiul Independentei 202, Bucharest-060021, Romania
- [c] Dipartimento di Chimica e Tecnologie Chimiche, Università della Calabria, via P. Bucci 14/c, 87030
- [d] Department of Chemistry, Syracuse University, Syracuse, NY 13244-4100, USA
- [e] Departament de Química Inorgànica/Instituto de Ciencia Molecular, Facultat de Química de la Universitat de València, C/ Catedrático José Beltrán, 46980 Paterna, València, Spain, E-mail address: miguel.julve@uv.es



(a)



(b)

**Figure S1.** FTIR spectra for compounds **1** (a) and **2** (b)

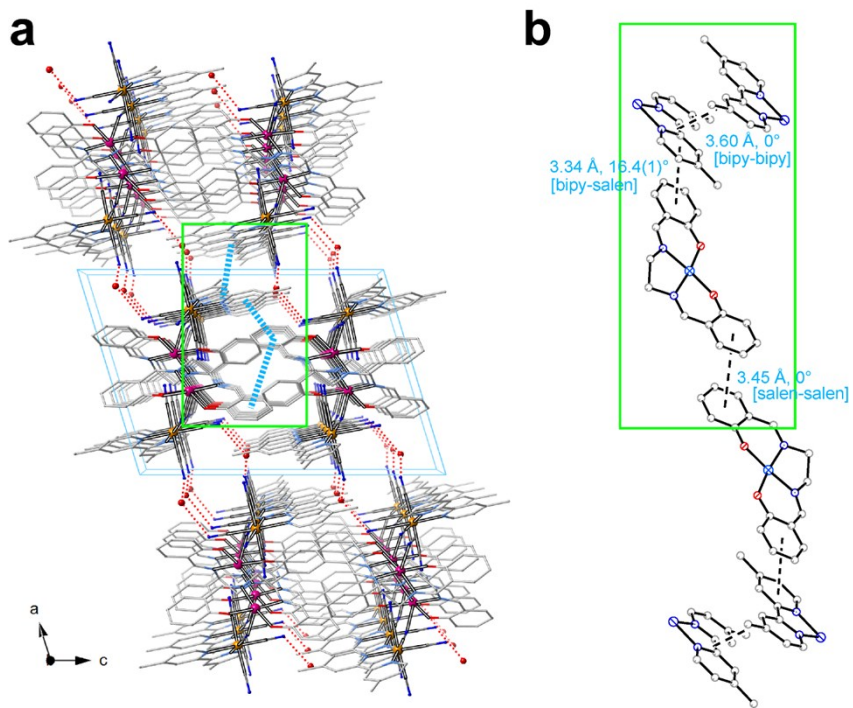


**Figure S2.** Perspective view of a fragment of the crystal packing of **1** along the crystallographic *b* axis (**a**), showing two adjacent supramolecular layers. Main inter-layer interactions, of the aromatic stacking type, are highlighted in (**b**).

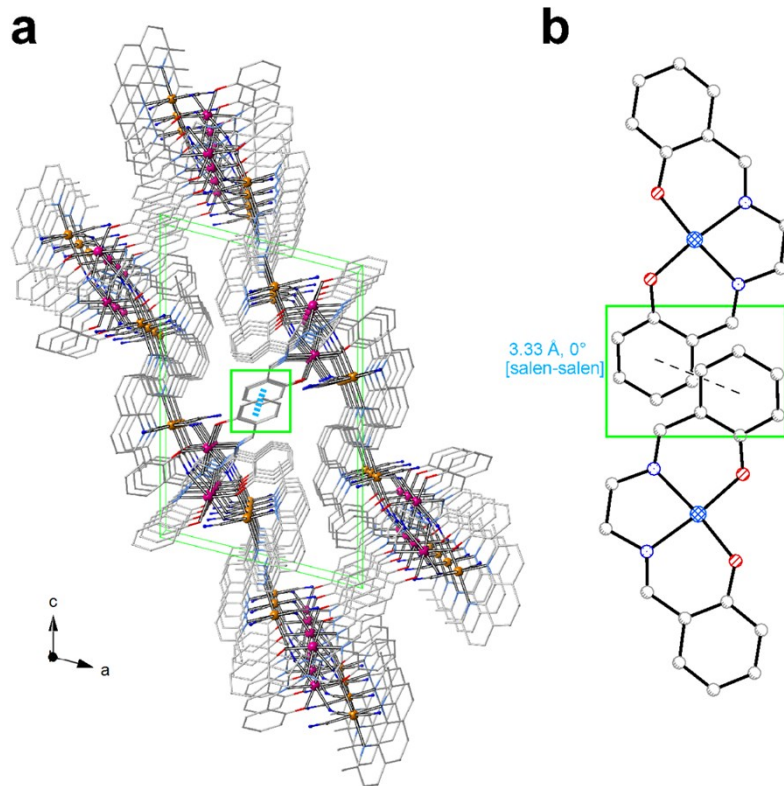


**Figure S3.** Perspective view of a fragment of the crystal packing of **2** along the crystallographic *b* axis (**a**), showing two adjacent supramolecular layers. Main inter-layer interactions, of the aromatic off-set stacking type, are highlighted in (**b**).

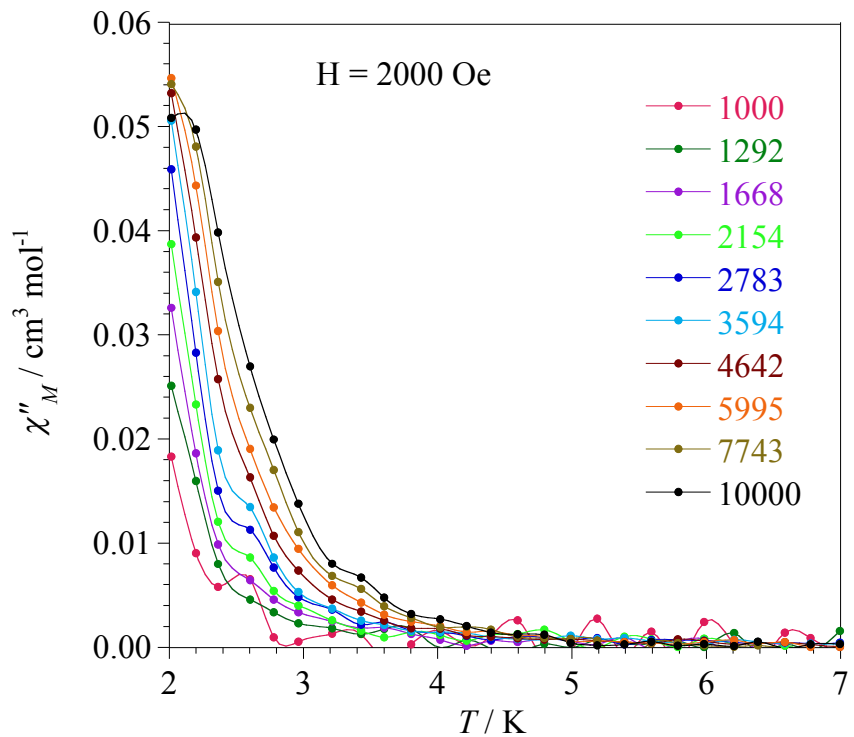
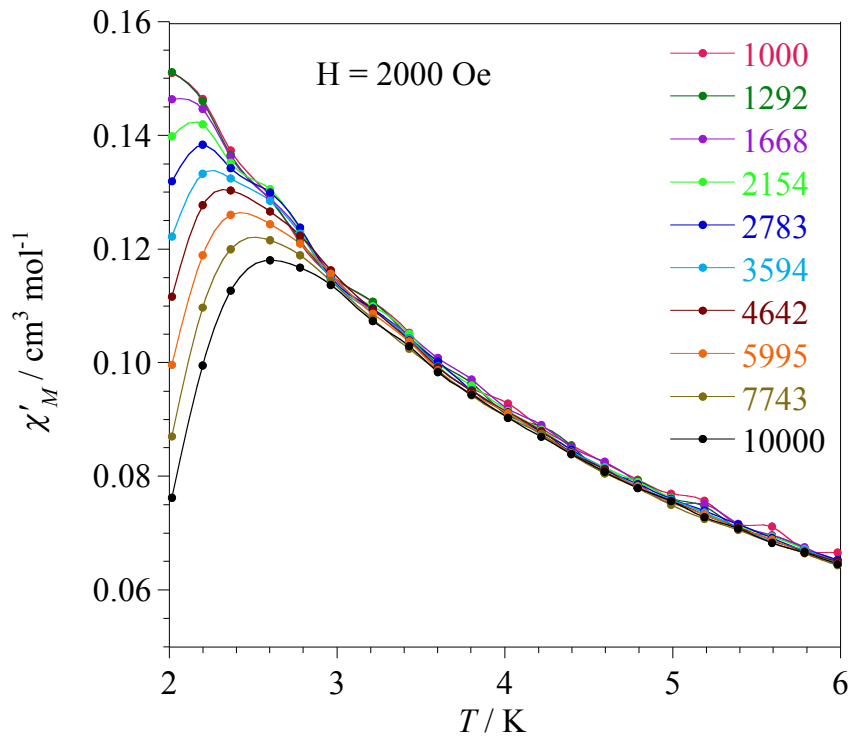


**Figure S4.** Frequency and temperature dependence of the in-phase magnetic susceptibility under external applied dc magnetic field of 2000 Oe in a  $\pm 4$  Oe oscillating field and in the frequency range 1000-10000 Hz for **2**.

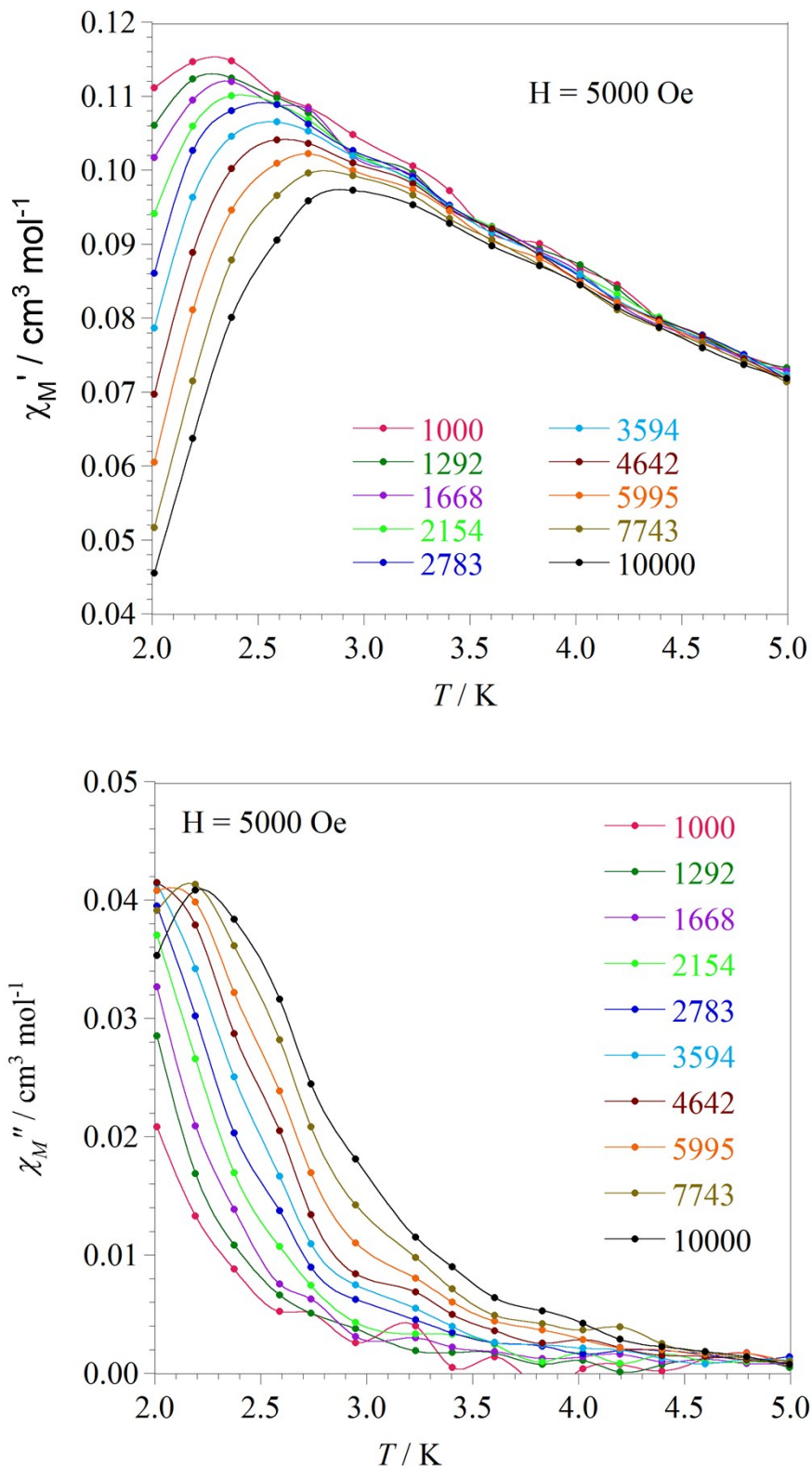


**Figure S5.** Frequency and temperature dependence of the in-phase magnetic susceptibility under external applied dc magnetic field of 5000 Oe in a  $\pm 4$  Oe oscillating field and in the frequency range 1000-10000 Hz for **2**.

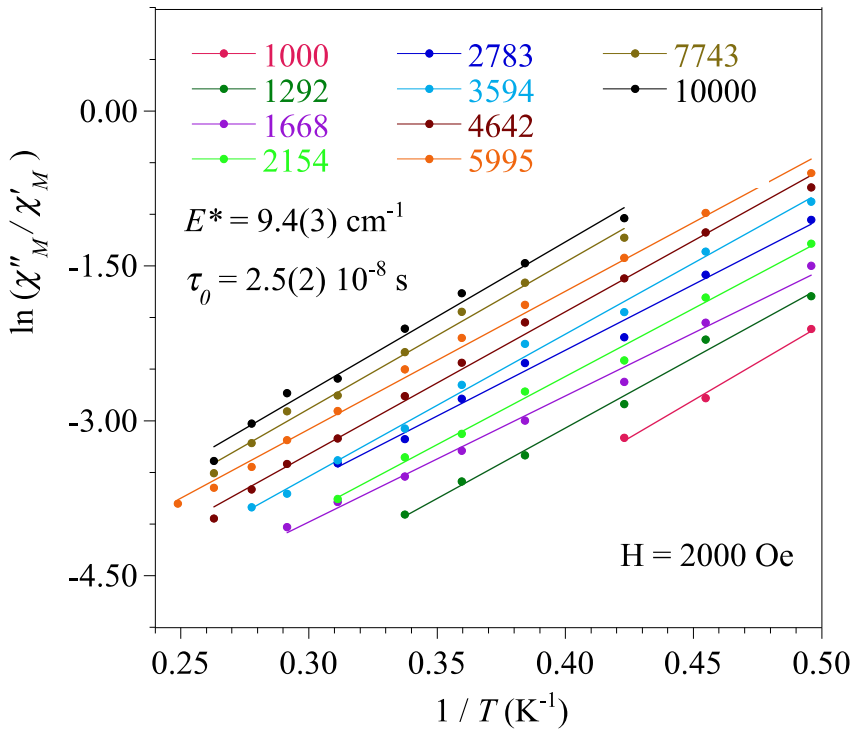


**Figure S6.** Natural logarithm of the ratio of  $\chi''_M$  over  $\chi'_M$  against  $1/T$  at ten different frequencies under external applied dc magnetic field of 2000 Oe, for **2**.

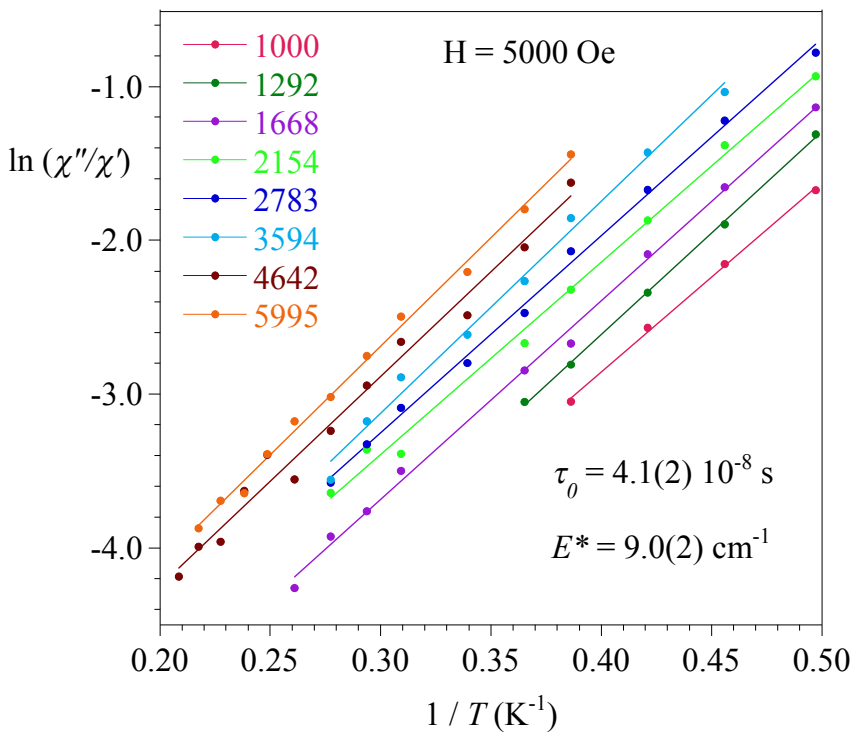


**Figure S7.** Natural logarithm of the ratio of  $\chi''_M$  over  $\chi'_M$  against  $1/T$  at eight different frequencies under external applied dc magnetic field of 5000 Oe, for **2**.

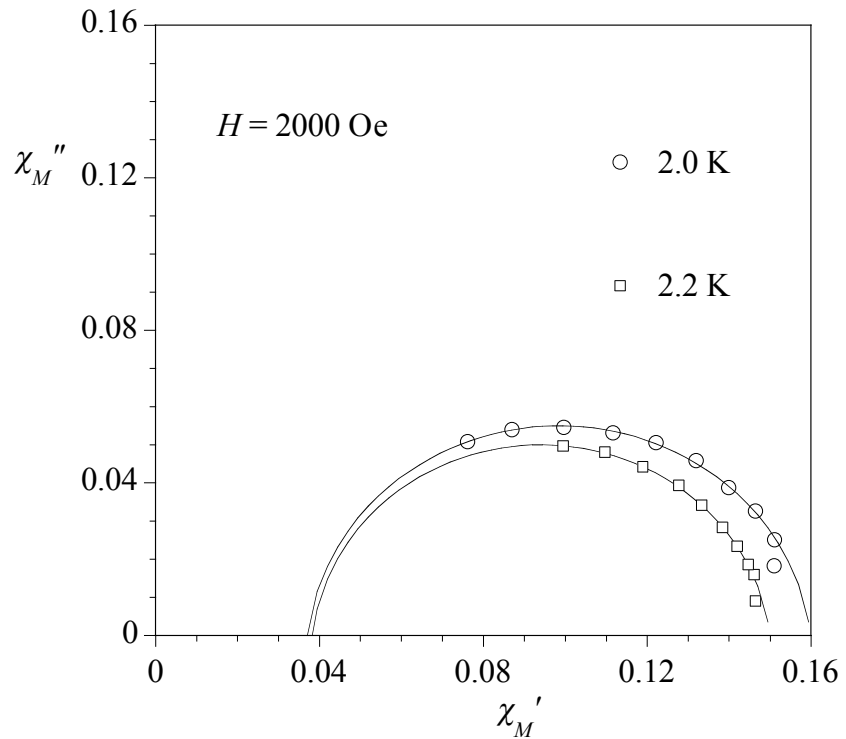


**Figure S8.** Cole-Cole plots for **2** under external applied dc magnetic field of 2000 Oe.

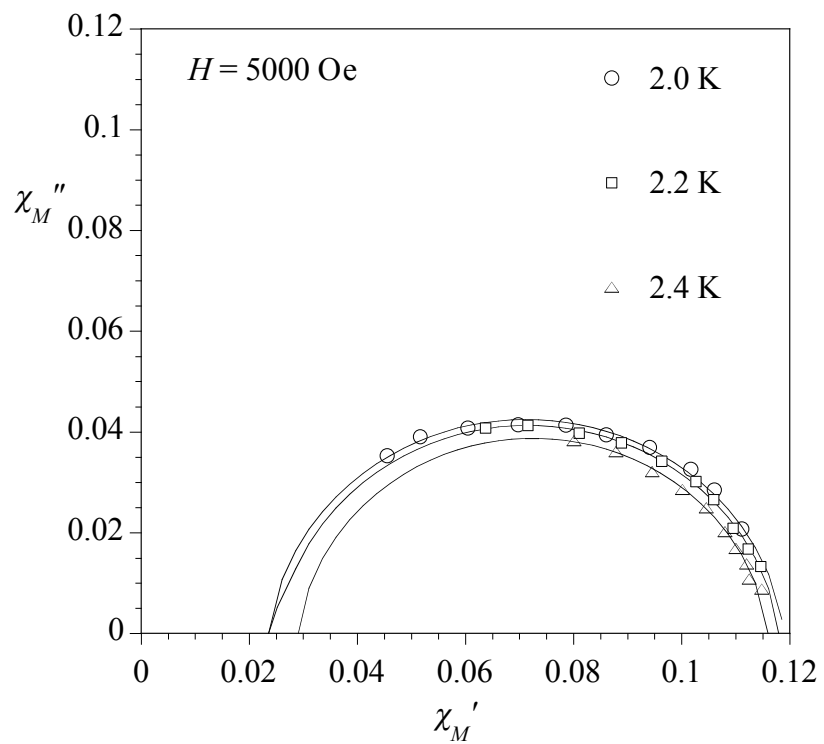


**Figure S9.** Cole-Cole plots for **2** under external applied dc magnetic field of 5000 Oe.

**Table S1.** Selected ac magnetic data for 2

$H_{dc}$ /Oe	T/K	$\alpha$	$\chi_s^a$ / cm <sup>3</sup> mol <sup>-1</sup>	$\chi_t^b$ / cm <sup>3</sup> mol <sup>-1</sup>
2000	2.0	0.071	0.037	0.16
2000	2.2	0.071	0.038	0.15
5000	2.0	0.074	0.024	0.12
5000	2.2	0.074	0.025	0.12
5000	2.4	0.073	0.029	0.12

<sup>a</sup> Adiabatic susceptibility. <sup>b</sup> Isothermal susceptibility.

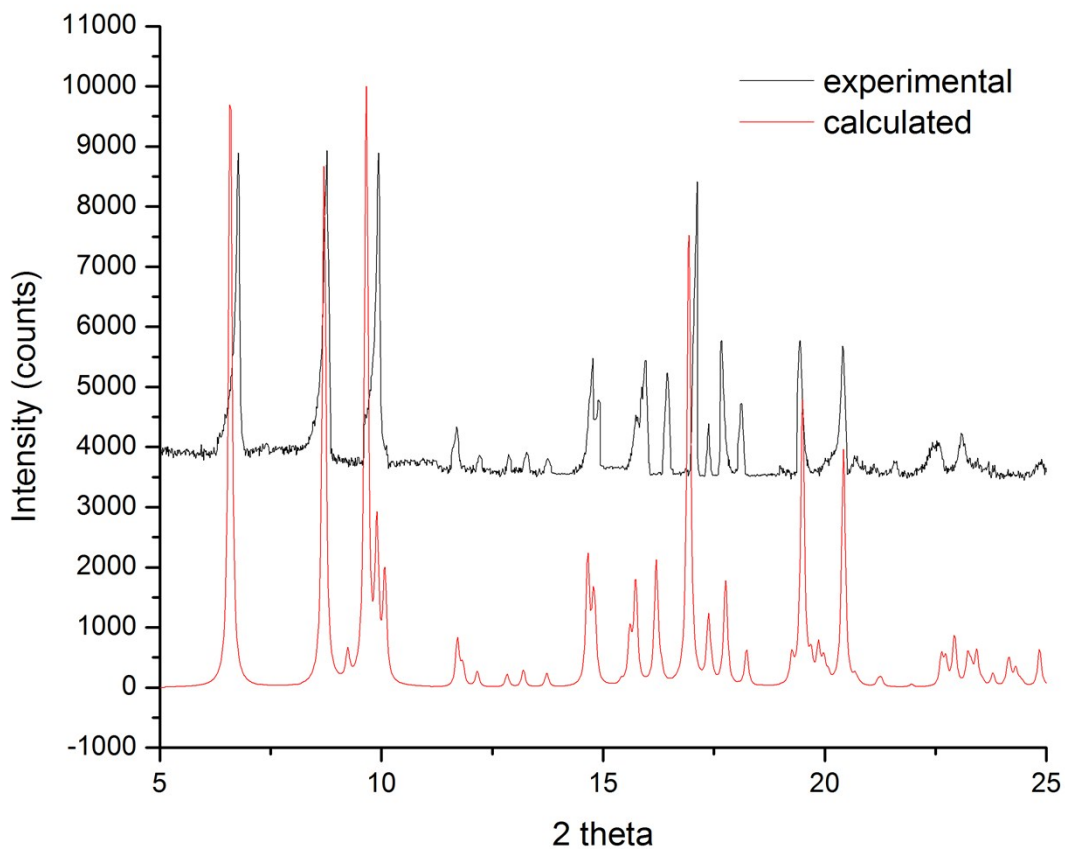


**Figure S10.** X-ray diffraction on powder for compound **1**: experimental (—) and calculated (—)

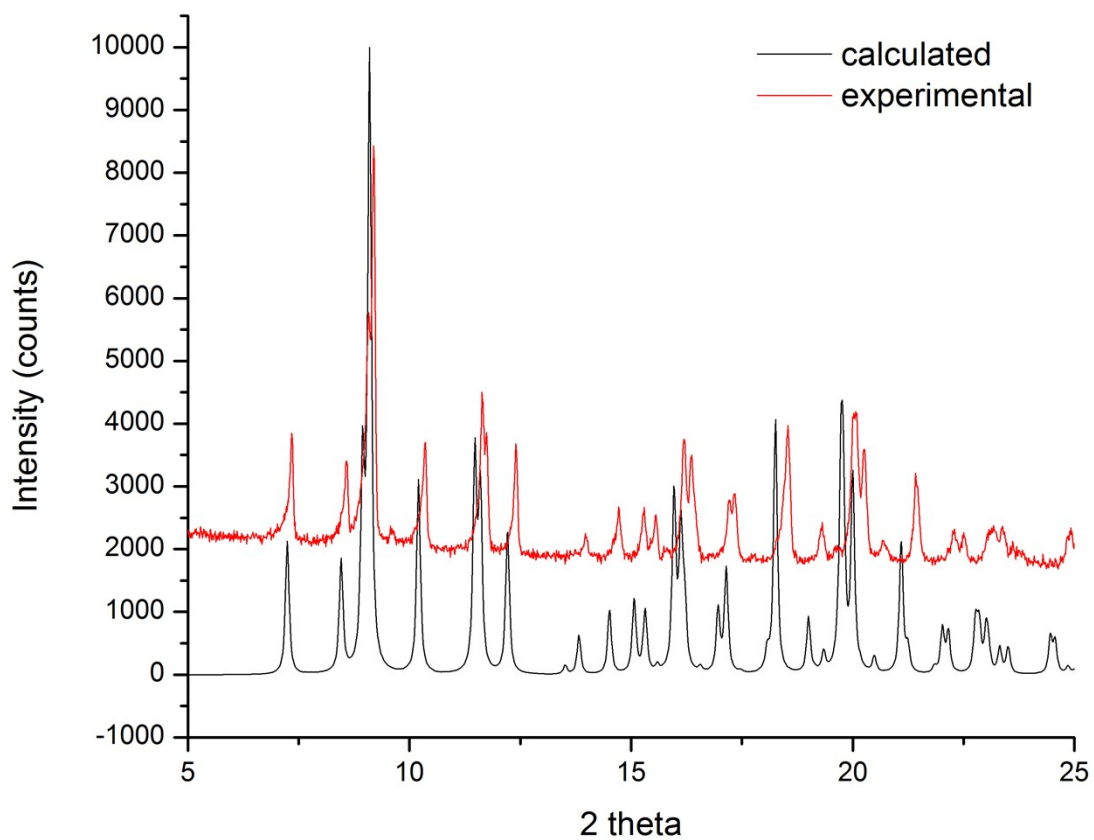


**Figure S11.** X-ray diffraction on powder for compound **2**: experimental (—) and calculated (—)